Photon detection at subwavelength scales

Wang, Q.

Author: Wang, Qiang
Title: Photon detection at subwavelength scales
Issue Date: 2015-10-27

Chapter 1

Introduction

1.1 Single photons and single-photon detection

In classical theories light is considered to be an electromagnetic wave that interacts with matter by driving the electrons of the constituent atoms. Such a description that uses either classical optics, or Maxwell's equations is proven to be highly successful and is most often sufficient for practical applications. However, these classical theories have great difficulty in explaining the photoelectric effect originally described by H. Hertz in 1887 [1]. The photoelectric effect is the observation that electrons are ejected from a metal provided that the frequency of the light exceeds a certain threshold. An elegant explanation of this effect was given by A. Einstein in 1905 [2], proposing that light consists of discrete wave packets with an energy equal to $\hbar\omega$, where ω is the angular frequency of the light and $\hbar$ is the reduced Planck constant.

These wave packets or quanta of light are commonly called photons and, for visible light, carry a discrete amount of energy of the order 10^{-19}J. This energy can be detected by extremely sensitive single-photon detectors that generate a "click" whenever detection takes place. The concept of photons as particles of light, the description of physical phenomena based on the statistical description of these particles and our ability to detect these particles with modern technology have lead to the development of the field of quantum optics. This field has been key to many scientific discoveries and has spawned multiple applications based on single-photon detector technology [3–5].

Our ability to detect single photons allows measuring light at extremely low levels, with applications in sensing [6], medical imaging [7], astronomy [8], thermal detection [9] and spectroscopy [10]. Naturally, it is extremely relevant when the quantum nature of light itself becomes important. For instance, the field of quantum information processing deals with the production, manipulation and detection of single photons with wide applications in quantum key distribution [11] and quantum random number generators [12]. High-speed, efficient detectors with low electronic jitter and low noise or dark count rate are essential to the development of these applications.

Traditionally, photo-multipliers and semiconductor avalanche photodiodes have been used for single-photon detection [5,13]. More recently, thin superconducting nanowires have been developed as a novel platform for single-photon detection [14]. These superconducting single-photon detectors (SSPDs) have become the prime candidate for demanding single-photon counting applications, exhibiting dark count rates below 10 s^{-1} [15], electronic jitter below 20 ps [16], detection efficiencies of more than 90% [17] and an extremely broad spectral range, extending to $\lambda = 5$ μm [18]. In addition, with proper electronic design, an array of SSPDs can be used to achieve photon number resolution [19] or for camera applications [20, 21].

Further technological improvements and use of these detectors require a better understanding of the photon-detection mechanism. Different detection models [14, 22–25] have been introduced that all contain assumptions that may or may not be valid for a specific choice of wavelength and superconducting material. Comparison of these models with experimental data on technologically relevant devices is difficult because these devices are based on long, meandering wires that introduce potential problems, such as current crowding in bends [26], fabrication errors and/or inhomogeneity in the superconductor [27].

In this thesis we aim to study the detection mechanism of NbN SSPDs using a simple device structure. It consists of a short section of superconducting wire made by nanofabrication techniques. To analyze the process of photon detection and to separate the internal, microscopic, detection efficiency from optical coupling efficiency we make use of a technique known as quantum detector tomography [28, 29] throughout this thesis. This method separates the response of the detector into distinguishable contributions of a well-defined photon number. Therefore we gain access to the energy or photon number dependence of the detection mechanism [30]. The wires studied in this thesis have typical dimensions that are smaller than the wavelength of light and hence the study of the details of the microscopic detection model takes place on a subwavelength scale.

Nano-sized SSPDs offer yet another new and exciting opportunity that is not possible with conventional detectors. Because of their nanoscale dimensions they can be used as a subwavelength probe in the optical near field to replace current near-field probes that all transport the radiation from the optical near field to a bucket style single-photon detector placed in the far field. A fundamental difference arises because the SSPD based probe is based on near-field absorption instead of scattering [31, 32]. In the second part of this thesis we study the possibility of subwavelength near-field probing with an SSPD to either probe nanoscale emitters or to explore the physics of the detection mechanism in a direct way using a near-field probe.

1.2 Superconducting single-photon detectors

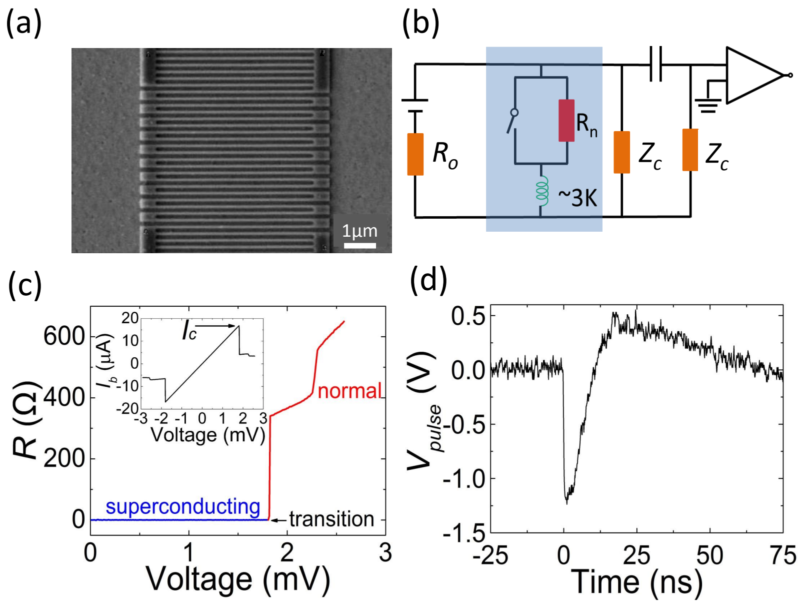

Figure 1.1: Various aspects of SSPDs. a) shows an SEM image of a meandering NbN SSPD on a GaAs substrate. (b) shows a schematic of the measurement circuit. The resistor of $R_o = 100\ \Omega$ is used for limiting the bias current. The electric model of the SSPD is shown in the light-blue area, which corresponds to the cryostat at a temperature of ~ 3 K. A photon detection event where the SSPD transits from the superconducting to the normal state after the absorption of a photon is equivalent to the switch going from closed to open. The bias current is diverted to $Z_c = 50\ \Omega$, which is the impedance of the BNC cable. As a result, a voltage pulse is transmitted to the amplifier and recorded by an electronic counter (not shown) as a count. (c) shows the dependence of the resistance of the detector as a function of the driving DC voltage. The blue line and red step-like curve indicate the superconducting and normal states, respectively. The inset shows the bias current as a function of the voltage output, and the maximum point corresponds the experimental critical current I_c. (d) shows a typical pulse with its polarity inversed after 60 dB amplification. The width of the pulse is about 5 ns and is limited by the detection electronics; this determines the reset time and maximum speed of the SSPD.

Throughout this thesis we use or investigate NbN SSPDs with the goal to gain a better understanding of photon detection at the nanoscale. These detectors consist of a thin and narrow strip of superconducting material to which a bias current is applied that is comparable to the critical current of the device. Under those conditions absorption of the energy of a single photon is sufficient to drive the nanowire from the superconducting state to the normal state. Once the wire is in a resistive state a voltage difference over the wire is generated that can be amplified and read out with pulse counting electronics.

Figure 1.1 introduces the basic concepts of single-photon detection with an SSPD. An SEM image of a meandering wire on a GaAs substrate is shown in Fig. 1.1(a)[1]. The NbN film with a thickness of $\sim$ 4 nm is first grown on a GaAs substrate by DC magnetron sputtering. Afterwards, the $\sim$ 100 nm wide meandering wire is defined through a procedure of electron beam lithography followed by reactive ion etching. During the fabrication, a HSQ (Hydrogen silsesquioxane) layer with a thickness of $\sim$ 80 nm is left on the wire.

An equivalent electronic circuit that explains the electronic operation of an SSPD and the photon counting mechanism is depicted in Fig. 1.1(b). The part of the circuit enclosed in the light blue area represents the equivalent circuit of the detector and is kept at a temperature of $\sim$ 3 K, well below the transition temperature of the superconducting material ($T_c \sim 10$ K for the thin NbN films used in this thesis). A constant bias current is supplied by the voltage source with a resistor $R_0 = 100\ \Omega$ in series. Figure 1.1(c) shows the measured resistance of the wire as a function of the applied voltage, showing the transition from the superconducting state to the resistive state. The inset shows the measured voltage as a function of bias current through the detector. The linear regime with a slope set by the resistor R_0 corresponds to the superconducting state that survives until the device critical current $I_c \approx 18\ \mu$A.

The equivalent circuit contains an inductance to represent the kinetic inductance of the current-carrying superconductor. Absorption of a photon that induces a transition from the superconducting state to the normal state is equivalent to opening of the switch to create a finite resistance value. The start of a resistive state of the current-carrying wire leads to additional Joule heating in the wire that drives part of the wire to the normal state with a resistance R_n of several kΩ. Once the detector is resistive the current is diverted to the load (cable) impedance $Z_c = 50\ \Omega \ll R_n$ where a voltage pulse is generated that is amplified by the amplifier. The characteristic timescale for this process is set by L_k/R_n, where L_k is the kinetic inductance set by the geometry and material properties of the superconductor [33]. Since the current through the SSPD is now reduced, its Joule heating stops and the SSPD becomes superconducting again. The current in the wire returns at a timescale $L_k/50\Omega$. For typical device dimensions $L_k \approx 100$ nH and the reset time of the detector is several nanoseconds.

A typical voltage pulse after amplification with a total gain $g = 60$ dB is

[1] The sample and image are provided by Eindhoven University of Technology

shown in Fig. 1.1(d). The negative polarity is a consequence of the internal details of the amplifier. The AC coupled amplifier creates a pulse with a response time of ~ 5 ns, which is limited by the speed of this detector-amplifier combination that couples the 50 Ω load impedance of the coaxial cable. It is important to note that most of the electric energy in the pulse is generated when the detector has returned to the superconducting state. This power is stored in the kinetic inductance of the superconductor. The energy in the pulse of Fig. 1.1(d) can be estimated as $(1/g^2)(V_p^2/Z_c)\tau = 2.8 \times 10^{-16}$ J $= 1750$ eV, where $g = 60$ dB $= 10^3$ is the total voltage gain of the amplifiers. This energy is 10^3 times larger than the energy stored in the photon and any information from the detection mechanism is erased in the process of generating the pulse. Chapters **3**, **4** and **7** of this thesis aim to understand the detection mechanism in SSPDs and use different methods: quantum detector tomography in Chapters **3** and **4**, and near-field optics in Chapter **7**.

1.3 Quantum detector tomography

Significant progress towards understanding the detection mechanism of SSPDs has been made through quantum detector tomography (QDT) [28, 34]. This method characterizes the response of the detector in an agnostic way allowing for unbiased physical interpretation. QDT has been applied to retrieve the intrinsic quantum response of SSPDs to different photon numbers [29, 35–37], which allows us to unravel the physics of the detection mechanism [30, 38].

To perform QDT, the detector is illuminated using a set of coherent states of different average powers. In the experiment these states are obtained by attenuating the output of a pulsed laser. In this way the total detection probability as a function of average input power is recorded. An algorithm that takes into account the photon number distribution of the coherent states used to probe the detector converts this information to an internal detection efficiency expressed in the photon-number or Fock-state basis. This completely describes the detector.

For single-photon detectors with low efficiency, many parameters are needed to completely describe the response of the detector in the photon-number basis [28]. Finding the number-basis representation corresponds to an inversion of coherent state statistics from the measured count rates and is an intrinsically ill-conditioned problem [28, 34]. To overcome this problem some amount of smoothing or regularization needs to be applied to avoid that small fluctuations in the measured data lead to large changes in the characterization of the detector [28]. In this thesis we implement this smoothing by noting that an attenuated coherent state remains a coherent state with a lower average photon number. We subsequently perform the tomography by separating the linear loss from the response in the number basis of photons absorbed by the detector instead of photons incident on the detectors [29].

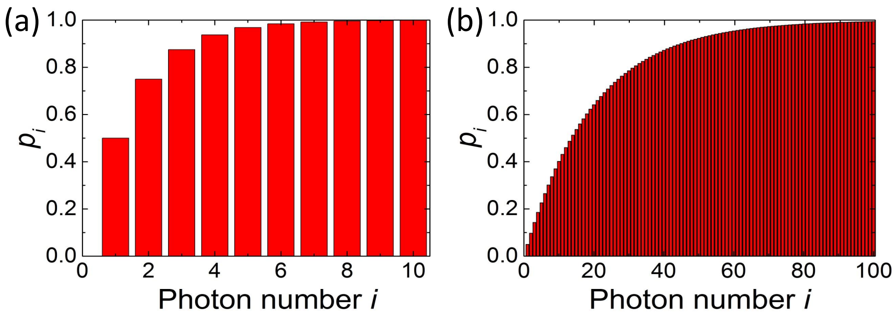

Figure 1.2: Detection probability p_i of an APD for i input photons. (a) and (b) show the probabilities that are required to describe the APD with values of single-photon detection efficiency p_1 equal to 0.5 and 0.05, respectively.

To illustrate this modified scheme, let us consider two avalanche photodiodes (APDs) a and b. We assume that the internal detection efficiencies for single-photon detection are $p_{a,1} = 0.5$ and $p_{b,1} = 0.05$, respectively. For APDs the multi-photon detection probability is known to be binomial [5, 13] and hence the detection probability for i photons is given by $p_i = 1-(1-p_1)^i$. The corresponding multi-photon detection probabilities are plotted in Fig. 1.2. Without prior knowledge of the operation of an APD (which is the purpose of QDT) about 10 probabilities p_i are needed to characterize the detector with 50% efficiency, while the 5% efficient detector requires 100 probabilities p_i. By factoring out the linear efficiency η in the modified tomography scheme we reduce the computational complexity from determining order η^{-1} parameters to less than 10 parameters.

The number of parameters that are needed to describe the operation of an SSPD depends on the experimental settings such as bias current and temperature. Noise in experimental data may reduce the amount of information that can be meaningfully extracted [34]. In Chapter **2** we investigate in detail the relation between the linear efficiency η and the internal detection efficiencies p_i for a meandering wire NbN SSPD and achieve an estimated relative uncertainty of 2%. We determine the influence of shot noise and four other technical noise sources on the outcome of quantum detector tomography, and we find that for long integration time (> 1 s) shot noise in the measured count rates no longer dominates the accuracy.

1.4 Photon detection mechanism of SSPDs

The question of how photons are detected in SSPDs, and in NbN based SSPDs in particular, is a scientific question that has been investigated since the discovery of single-photon detection by an SSPD [14]. As an initial model, a "hotspot" has been introduced where a core of normal material is created that diverts the supercurrent around the normal-state material. As a result the current density locally exceeds the critical current density and a detection event occurs. While this detection model should prevail for very large excitation energies [39], experiments show that this model fails to explain data for photon energies of a few electron volts (visible and near-infrared wavelengths) [30]. Most notably, the hotspot model predicts a nonlinear energy-current relation and a sharp transition in the count rate as a function of bias current because detection events are impossible below a certain current density [40].

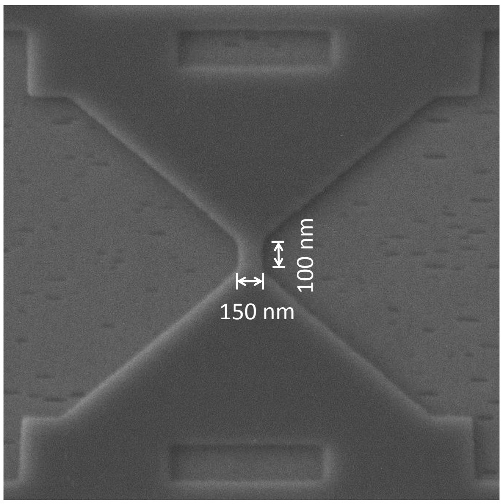

Figure 1.3: SEM image of a NbN single wire SSPD. A $\sim$ 4nm thick, 150 nm wide and 100 nm long nanowire in between two tapered parts is fabricated on a GaAs substrate.

An important and open question in the field of SSPDs is thus the microscopic detection mechanism that causes photon detection. Understanding of the microscopic mechanism may help to design better detectors and is essential when operating these detectors in quantum-optical experiments. Various models have been proposed as an alternative to the hotspot model to describe the interaction between light and a current-carrying superconducting nanowire [22–25]. The challenge remains to perform experiments that either confirm or exclude a specific model. So far, a linear dependence of the internal detection efficiency p_i as a function of photon energy has been found for NbN detectors in the energy range from 0.7–8 eV [30]. These measurements use the modified quantum detector tomography (as outlined in the previous section and Chapter **2** of this thesis) and are consistent with a detection model that involves photon-assisted vortex entry [25].

Our current understanding of the detection mechanism based on photon-assisted vortex entry implies that the response of the detector depends on the position where the photon has been absorbed. Controlled experiments with a simple detector geometry are needed to investigate the photon detection mechanism on the nanoscale. Figure 1.3 shows an SEM image of a short NbN single wire in between two tapered contact areas, nominally identical to the sample used in Chapter **3** of this thesis[2]. For this simple geometry, the active area is the short wire section and issues with current crowding due to bends [41] and inhomogeneities that reduce the critical current in a long wire [27] are largely avoided. As we show in Chapters **3** and **4** the optical response of this short section of wire is identical to that of the meander and can be calculated numerically using the known dielectric constant of NbN. Hence, tomography performed on this wire comprises a measurement of the linear, effective absorption efficiency η and the internal detection efficiencies p_i.

In Chapter **3** we demonstrate that the measured values of p_i together with the calculated electromagnetic field distribution in the wire comprise a method to experimentally probe the spatial variation in the detection efficiency within the wire. The field distribution in the wire is due to the properties of the material and boundary conditions depending both on polarization and wavelength of the incident light. Because the measured internal detection efficiencies depend on polarization of the incident light, this immediately implies that the internal efficiencies p_i are position dependent. We find that the edges of the wire are much more effective than the center, and that high detection efficiencies are achieved for distances $\sim$ 30 nm form the edge. Our result is logically consistent with the model of photon-assisted vortex entry [25].

To illustrate that the local detection efficiency determined in Chapter **3** is technologically relevant we calculate the polarization-dependent response of various meandering nanowire structures and compare these to experimental results from Anant et al. [42] in Chapter **4**. These calculations show that the internal detection efficiency of meandering wire structures is less than 100% for typical bias currents and wire widths used for state-of-the-art devices. The model detailed in Chapter **3** allows us to explain some intrinsic features that were hitherto not understood.

[2]The sample and image are provided by Eindhoven University of Technology

1.5 Subwavelength microscopy with nano SSPDs

Two essential experimental steps towards a detailed understanding of the photon detection event in SSPDs have been made in Chapters **2–4** of this thesis, namely the use of quantum detector tomography combined with the simplest possible detector geometry. Armed with the newly obtained knowledge, questions arise if these detectors can be probed via near-field scanning microscopy and whether the nanoscale detectors can be used as a near-field probe. We investigate these questions in detail in Chapters **5**, **6** and **7**.

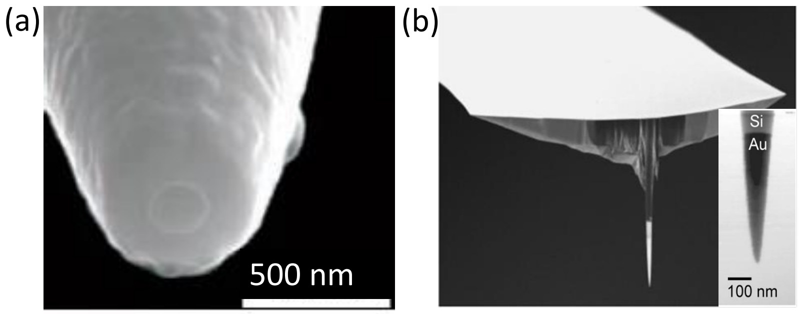

Figure 1.4: Two examples of SNOMs used by other groups. (a) shows the aluminum-coated probe of an aperture-SNOM [43]. The diameter of the aperture is about 200 to 230 nm. (b) shows the single gold tip attached to a silicon cantilever used in a scattering-SNOM [44].

Subwavelength imaging can be realized by scanning near-field optical microscopes (SNOMs), which beat the standard diffraction limit of conventional optical microscopes by scattering a small part of the optical near field to a large optical detector in the far field. Two methods for scattering the near field to a far-field detector have been developed. Figure 1.4(a) shows an example of an aperture based SNOM (a-SNOM) where light is scattered through an aperture into an optical fiber [45]. In the example, the fiber is coated with a 150 nm thick aluminum film and the subwavelength aperture has a diameter of 200–230 nm [43]. Figure 1.4(b) shows a tip on a cantilever used to realize what is called a scattering-SNOM (s-SNOM) [44]. The end of the sharp tip of a silicon cantilever is coated with gold (see inset of Fig. 1.4(b)). When illuminated from the side the optical response of this tip concentrates the electromagnetic field at the apex of the tip. When such a tip is placed in close vicinity of a sample, the optical near field is scattered by the tip and can be collected by a far-field detector.

Conventional SNOMs are intrinsically inefficient because they attempt to resolve subwavelength features using the physical mechanism of light scattering, which is characterized by strong size and wavelength dependence of the scattering efficiency. For scatterers much smaller than the wavelength, the Rayleigh limit applies and scattering cross section of the aperture or the tip apex is proportional to a^6/λ^4, where a is the size of the scatterer and λ is the wavelength of light [31]. A resolution of $\sim\ \lambda/10$ requires $a/\lambda \sim\ 0.1$, lowering the efficiency of the detector per unit area by 4 orders of magnitude. This low efficiency severely limits the application of SNOMs to quantum optics because the optical loss associated with the low efficiency erases the underlying photon statistics of non-classical light [46].

In Chapter **5** we explore the possibility to use a nanoscale NbN SSPD as an efficient probe based on the experimental observation of a working detector of $50\times50\ \mathrm{nm}^2$ size. Because of the strongly absorbing nature of NbN material [47], characterized by the dominant imaginary part of the dielectric constant, this probe functions as a near-field absorber that is capable of detecting single photons. To estimate the performance of this novel near-field probe we calculate the interaction between a radiative dipole source and the detector. Both the detection efficiency and the influence on an emitter is compared to that of a SNOM probe made out of a well-conductive metal such as gold or silver. We find that the absorption cross section proportional to a^3/λ (a is the dimension of the nanoscale SSPD) is at least two orders of magnitude higher than the scattering cross section in SNOMs while the influence on the properties of the emitter are less than that of conventional SNOMs.

To directly measure the nanoscale response of an SSPD with the aim to independently confirm the detection model we design a scattering tip based SNOM. The design of the scattering tip above the NbN detector is detailed in Chapter **6** that discusses the influence of the tip geometry on the localization of field at the tip apex. The field localization of a tip with finite length is due to a plasmonic resonance in combination with a singularity or lightning-rod effect at the apex [48, 49]. We determine the role of this resonance in the absorption of the detector and determine the perturbing effect of a resistive load due to the detector in the near field of the antenna (tip). We find that the absorption of the detector as a function of wavelength is qualitatively similar to the field enhancement calculated for a tip without detector if the distance between tip and sample is comparable to the radius of curvature of the tip apex.

To resolve the local detection efficiency, an s-SNOM with a spatial resolution better than $\sim$ 30 nm needs to be designed based on the results of Chapter **4**. This resolution is outside the regime of conventional aperture based SNOMs because this length scale is smaller than twice the skin depth in metals used as a cladding material of the fiber tip. Calculations in Chapter **7** show that a realistic design of a tip leads to an s-SNOM with the desired resolution and we calculate the expected response of the detector when illuminating the tip-detector system from the side. We observe that the detector response exhibits two narrow peaks on the edge of the nanowire due to the distribution of both optical absorption and internal detection efficiency near the edges. Realizing this configuration in an actual experiment will give valuable information on the detection mechanism, and holds promise for new applications in near-field optics. For instance a nanodetector that is efficiently coupled to a tip could be used as an efficient multi-photon detector that samples the statistics of various quantum states of light.